# UC San Diego
## UC San Diego Previously Published Works

**Title**

Infusible Extracellular Matrix Biomaterial Promotes Vascular Integrity and Modulates the Inflammatory Response in Acute Traumatic Brain Injury.

**Permalink**

**Journal**

**Authors**

Diaz, Miranda

Kandell, Rebecca

Wu, Jason

et al.

**Publication Date**

**DOI**

Peer reviewed

# Infusible Extracellular Matrix Biomaterial Promotes Vascular Integrity and Modulates the Inflammatory Response in Acute Traumatic Brain Injury

Miranda D. Diaz, Rebecca M. Kandell, Jason R. Wu, Alexander Chen, Karen L. Christman,* and Ester J. Kwon*

Traumatic brain injury (TBI) affects millions of people each year and, in many cases, results in long-term disabilities. Once a TBI has occurred, there is a significant breakdown of the blood—brain barrier resulting in increased vascular permeability and progression of the injury. In this study, the use of an infusible extracellular matrix-derived biomaterial (iECM) for its ability to reduce vascular permeability and modulate gene expression in the injured brain is investigated. First, the pharmacokinetics of iECM administration in a mouse model of TBI is characterized, and the robust accumulation of iECM at the site of injury is demonstrated. Next, it is shown that iECM administration after injury can reduce the extravasation of molecules into the brain, and in vitro, iECM increases trans-endothelial electrical resistance across a monolayer of TNF$\alpha$-stimulated endothelial cells. In gene expression analysis of brain tissue, iECM induces changes that are indicative of downregulation of the proinflammatory response 1-day post-injury/treatment and neuroprotection at 5 days post-injury/treatment. Therefore, iECM shows potential as a treatment for TBI.

## 1. Introduction

Over 2.7 million Americans experience traumatic brain injury (TBI) each year.[1] Groups at increased risk for TBI include ethnic or racial minorities, those experiencing homelessness, children, and military members.[2] Currently, the standard of care for patients suffering from TBI is emergency medicine at the acute stage, which involves monitoring for internal bleeding, swelling, and oxygen supply, and palliative care at the chronic stage. However, there are no therapeutics available that can mitigate the progression of injury or promote repair of the damaged tissue. The initial trauma of TBI causes vascular and tissue damage from the physical impact. From minutes to months afterward, a secondary injury progresses throughout the perilesional region surrounding the injury and includes sustained dysfunction of the blood-brain barrier (BBB), neuroinflammation, and neuronal cell death.[3,4] Of particular interest to this study is the increased permeability of the BBB, which leads to increased extravasation of blood components into the brain,[5–7] leading to detrimental effects on the perilesional tissue such as edema, immune infiltrate, and toxic levels of blood components in the brain, ultimately contributing to the progressive deterioration of nervous tissue.

Decellularized extracellular matrix (ECM) derived biomaterials have been applied to promote repair and mitigate the inflammatory response in various disease and injury models, such as myocardial infarction (MI), peripheral artery disease, and volumetric muscle loss.[8–11] These ECM biomaterials include injectable hydrogels, which require direct injection into the tissue of interest or, more recently, infusible ECM biomaterials that can be delivered via intravenous (i.v.) injection.[12] Previous studies have investigated the use of a brain ECM-derived hydrogel injected into the injury for the treatment of TBI, resulting in reduced lesion size, improved sensorimotor and cognitive performance, and amelioration of the neuroinflammatory response.[13] However, direct injection of a biomaterial into the brain is unfavorable for many patients as this would be an invasive surgical procedure that is resource-intensive and thus can potentially increase morbidity and delay treatment; it is known that reducing the interval between injury and treatment in TBI is associated with improved outcomes.[14] Therefore, an i.v. infusible biomaterial that can be delivered quickly after injury is more broadly applicable to different patient care settings. In order to create an ECM biomaterial that can be administered through a minimally-invasive injection, we previously developed an intravascularly

M. D. Diaz, R. M. Kandell, J. R. Wu, A. Chen, K. L. Christman, E. J. Kwon
Shu-Chien Gene Lay Department of Bioengineering
University of California San Diego
La Jolla, CA 92093, USA
E-mail: christman@eng.ucsd.edu; ejkwon@ucsd.edu
M. D. Diaz, R. M. Kandell, J. R. Wu, A. Chen, K. L. Christman, E. J. Kwon
Sanford Consortium for Regenerative Medicine
La Jolla, CA 92037, USA

ADVANCED
SCIENCE NEWS
www.advancedsciencenews.com

ADVANCED
HEALTHCARE
MATERIALS
www.advhealthmat.de

infusible decellularized ECM (iECM) derived from fractionating a digested myocardial ECM hydrogel that preferentially localizes to leaky microvasculature in regions of inflammation, including in MI and pulmonary arterial hypertension.[12] In a model of acute MI, intracoronary infusion of iECM improved cardiac function, reduced vascular permeability, promoted cardiomyocyte survival, and modulated the inflammatory response,[12] but no studies have fully evaluated targeting, dosing, and/or efficacy following systemic i.v. delivery or for the application to the BBB and TBI. While some studies suggest a tissue-matched ECM may be most effective for tissue regeneration,[8,15–17] in this study, we evaluated cardiac-derived ECM due to the difficulties and low yields in processing decellularizing brain ECM, which would make large-scale manufacturing challenging.[15] Further, a mass spectrometry organ ECM atlas has recently shown that while the ECM content of the brain is the most diverse out of any organ, the ECM content of the heart is among the most similar to that of the brain.[18] Notable differences found between brain and heart structural ECM proteins include the lowest content of fibrillar collagen in the brain, enrichment of multiplexins in the heart, and network-forming collagens in the brain. Based on their similarity, we reasoned that cardiac-derived iECM, which can be easily manufactured[12] and is derived from a myocardial ECM hydrogel that has been tested in patients,[19] could have a potential benefit for treating injuries in the brain.

In this study, we aimed to understand the feasibility and efficacy of administering iECM for the acute treatment of TBI in a mouse controlled cortical impact (CCI) model. Initially, we characterized the systemic half-life and retention of iECM in the injured mouse brain following single and multiple i.v. doses. We found that iECM accumulated into the injured brain in a dose-dependent manner where it colocalized with vasculature in the perilesional tissue. With a rapid intravenous half-life of ~5 min, iECM was retained in the brain for up to 3 days post-injection. Further, the redosing of mice significantly improved iECM brain signal over a single dose regimen. In the evaluation of the impact of iECM on BBB integrity, i.v. administered iECM attenuated the extravasation of 10 kDa dextran and bovine serum albumin (BSA) tracers. In vitro, iECM improved trans-endothelial resistance (TEER) of endothelial monolayers. Finally, through medium throughput gene expression, we show that iECM modulates pathways of neurodegeneration and neuroinflammation at both days 1 and 5 post-injury. This study is the first investigation into the efficacy and mechanism of action of an ECM-derived infusible biomaterial to promote repair after TBI and provides insight into a promising biomaterial for the treatment of TBI patients.

## 2. Results & Discussion

### 2.1. Fabrication and Characterization of iECM

The iECM has previously been shown to localize in regions of injury for several disease models.[12] In this study, we chose to investigate the iECM in a traumatic brain injury (TBI) mouse model. First, the iECM was fabricated and documented as previously described[12] (**Figure 1**a–g) and characterized in vitro to ensure the reproducibility of the iECM compared to the original fabrication of iECM. To ensure the reduction of high molecular

weight proteins, the lyophilized iECM was analyzed on an SDS-PAGE gel (Figure 1h) and compared to rat tail collagen type I, protein ladder, and the full ECM hydrogel from the same batch of hearts. To ensure injectability, the complex viscosity of the iECM was measured and shear thinning behavior was observed (Figure 1i). Further, the absorbance (Figure 1j) and transmittance (Figure 1k) curves of iECM resembled the saline control. Cryogenic transmission electron microscopy (CryoTEM) demonstrated the nanofibrillar architecture of the iECM (Figure 1l). Finally, the iECM underwent our standard quality control techniques, including double-stranded DNA quantification (0.35 +/− 0.09 ng mg$^{-1}$ of ECM) to ensure sufficient decellularization and sulfated glycosaminoglycans (sGAG) quantification, showing some residual sGAGs (0.47 +/− 0.08 µg mg$^{-1}$ of ECM).

### 2.2. iECM Accumulates in a Dose-Dependent Manner and Colocalizes with Brain Endothelium after Intravenous Delivery in a TBI Mouse Model

After the quality control validation of our fabricated iECM, we sought to determine whether systemically administered iECM was able to locate to the injured brain in a dose-dependent manner. iECM was labeled with the near-infrared fluorophore VivoTag 750 and injected at 25, 50, and 100 mg kg$^{-1}$ through the tail-vein 4 h after a controlled cortical impact (CCI). Brains were harvested after perfusion 1 h after iECM administration and the surface fluorescence from whole brains was imaged with a LiCor Odyssey (**Figure 2**a). We observed that the iECM localized to the injured hemisphere of the brain at all doses administered (Figure 2b). Additionally, whole brain scans show a clear dose-dependent accumulation of material in the injured region. Quantitative analysis of fluorescently-labeled iECM signal shows a significant increase in material accumulation at the 100 mg kg$^{-1}$ dose compared to all other doses of iECM (Figure 2c). While we have likely not reached maximum accumulation at 100 mg kg$^{-1}$ based on the linear increase in signal observed across doses, the maximum dose for a single injection is 100 mg kg$^{-1}$ due to the optimized concentration of the iECM and the limitations in the maximum volume for i.v. injections in mice. Due to this limitation in rodents, ultimately, dose optimization will need to be performed in a large animal model. To characterize the tissue-level localization of iECM, we injected Alexa Fluor 568-labeled iECM at 100 mg kg$^{-1}$ 4 h after injury and harvested brains 1 h post-injection. Tissue sections stained for CD31 show colocalization of iECM and endothelial cells as well as binding along microvasculature in the injury (Figure 2d). Additionally, we performed the same analysis after injection of an Alexa Fluor 568-labeled trilysine (Lys-Lys-Lys) control to confirm the specific localization of labeled iECM in the injured tissue. As expected, we observed some diffuse trilysine peptide in the injured region, but the signal was minimal and not colocalized with the vasculature (Figure 2e).

### 2.3. iECM Shows Clearance from Circulation and Retention in Injured Brain

Further analyses were done to understand the pharmacokinetics of iECM in the mouse model of TBI; we measured the blood
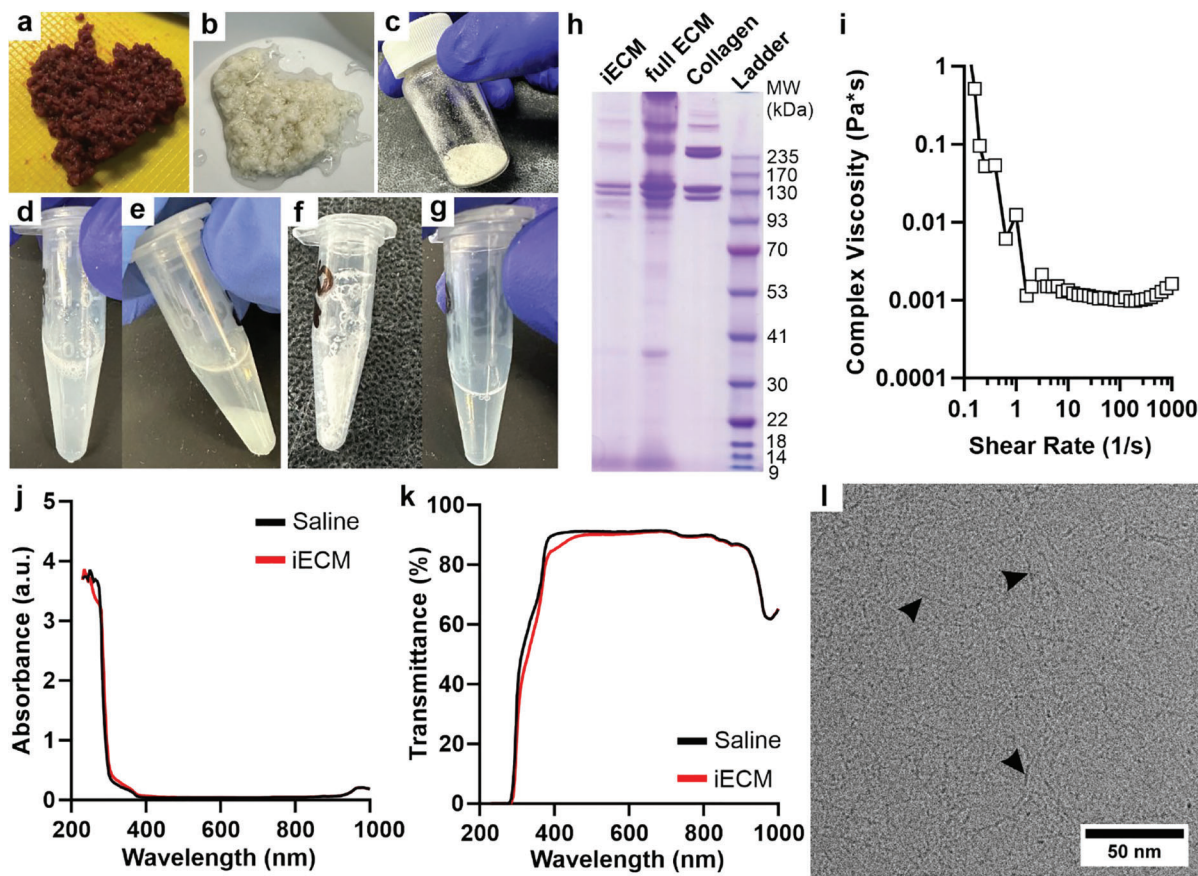
**Figure 1.** In vitro characterization of infusible ECM (iECM). a–g) Images of iECM fabrication process. a) Freshly chopped porcine myocardium. b) Decellularized ECM. c) Milled ECM. Digested ECM d) before and e) after centrifugation. f) Processed and lyophilized supernatant. g) Resuspended iECM pre-injection. h) SDS-PAGE of iECM, full ECM, and collagen. i) Complex viscosity of iECM. j,k) Absorbance and transmittance of iECM and saline. l) CryoTEM image of iECM (scale bar = 50 nm). Arrows note nanofibrous structure.

half-life of iECM in the systemic circulation and the time course of iECM retention in the injured brain and satellite organs. This was performed to understand how long the iECM is retained in the brain to better determine time points for assessing any possible functional benefits. Blood was sampled over 1 h after injection, and the blood half-life of iECM was measured as 5.6 min, indicating that iECM is rapidly cleared from the bloodstream (**Figure 3**a). We then harvested brains and satellite organs at 1 h, 6 h, 1 day, and 3 days after iECM administration. Brain surface imaging and fluorescence quantification showed iECM accumulation and retention in the injury that was detectable up to 1 day (Figure 3b,c). Additionally, analysis of the lungs, liver, kidney, spleen, and heart show that the iECM accumulates in the liver and kidneys 1 h after injection, but the signal rapidly diminishes over time (Figure S1, Supporting Information), suggesting iECM is likely efficiently eliminated through the urine and liver.

### 2.4. Multiple Doses of iECM Can Be Administered to Increase Brain Accumulation

As discussed above, while 100 mg kg$^{-1}$ was the maximum dosage for a single i.v. injection, maximum brain accumulation was likely not achieved at this dose (Figure 2b,c). Therefore, we in-

vestigated whether increases in accumulation could be achieved with multiple applications of the 100 mg kg$^{-1}$ dose. Based on iECM pharmacokinetic characterization (Figure 3), the blood half-life of iECM is on the order of minutes and the brain half-life of iECM is on the order of hours, although iECM can still be detected in the brain at 1 day. We thus investigated two different dosing regimens for two i.v. injections of iECM: 1) 30 min and 1 h post-CCI and 2) 30 min and 4 h post-CCI and compared the two dose regimens against a single dose administered at 30 min post-CCI (**Figure 4**a). Whole brain imaging and quantification revealed that both two dose regimens resulted in ≈2-fold increases in accumulation of iECM into the injured brain compared to a single dose of iECM, although the regimen of 30 min and 1 h post-CCI resulted in more consistent increases in accumulation (Figure 4b,c). Additionally, whole organ scans show that the material likewise increased in satellite organs when comparing the re-dose and single dose regimen (Figure 4d).

### 2.5. iECM Reduces Vascular Permeability In Vivo and In Vitro

During the period of BBB dysfunction, circulating proteins and proinflammatory cells accumulate in the injured brain, which drives the progression of the secondary injury.[20] Disturbance of
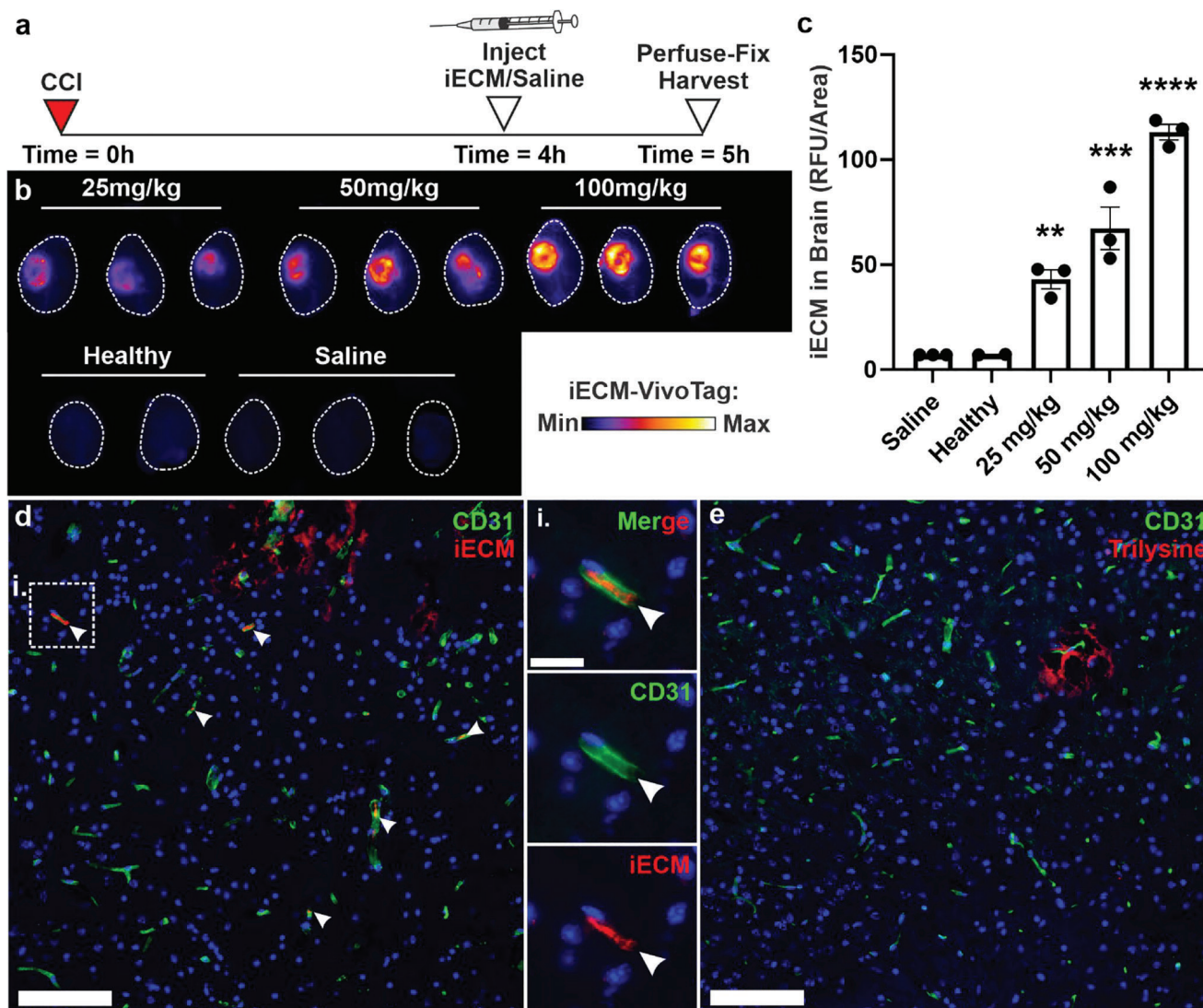
**Figure 2.** Dose-dependent accumulation of iECM in the injured brain after systemic administration. a) Timeline of dosing study. b) Whole brain fluorescence of iECM and c) quantification of these scans show the highest amount of iECM localization at 100 mg kg$^{-1}$ of iECM ($n = 3$ except for $n = 2$ for healthy control, mean $\pm$ SEM, **** $p < 0.0001$, *** $p < 0.001$, ** $p < 0.01$ ordinary one-way ANOVA with Dunnett's multiple comparisons test compared to saline). d) Labeled iECM or e) trilysine control with CD31-labeled endothelial cells in the injured region (blue, nuclei; green, CD31; red, AF568-labeled iECM or trilysine; scale bar = 100 μm). i) 40× magnification inset shows iECM colocalized with CD31$^{+}$ microvasculature (scale bar = 20 μm). Arrows note instances of iECM and CD31 colocalization.

the BBB results in swelling or edema, which can drastically increase intracranial pressure and increase the risk of tissue damage or death. For these reasons, there has been a recent focus on therapeutics that reduce vascular permeability in TBI.[21,22] Specifically, early intervention with therapeutics that reduce BBB permeability has been shown to reduce edema, improve sensorimotor functional outcomes, and modulate microglia activation and neuroinflammation in the brain.[23–25] Therefore, our next goal was to determine the effects of the iECM on vascular permeability. In previous applications of the iECM in acute MI, the material reduced the vascular permeability of albumin in the infarct region, which provided motivation for the application of iECM for mitigating increased vascular permeability and BBB dysfunction in TBI.[12]

To determine the effects of the iECM on vascular permeability in vivo, we measured the extravasation of two molecular weight tracers after i.v. delivery of iECM or saline in CCI-injured mice. Initial vascular permeability studies with the injection of iECM at 4 h post-injury trended towards a reduction in vascular permeability for iECM-treated mice, but the differences were highly variable (Figure S2, Supporting Information). Therefore, for all subsequent experiments, we investigated the acute application of iECM, where the iECM was injected 30 min post-injury to maximize the impact on vascular permeability. For this study, two different molecular weight tracer agents were used: 10 kDa dextran and 66.5 kDa BSA. The 10 kDa dextran is a polysaccharide tracer commonly used to evaluate BBB integrity, while BSA is representative of blood proteins known to cross the BBB after TBI, such
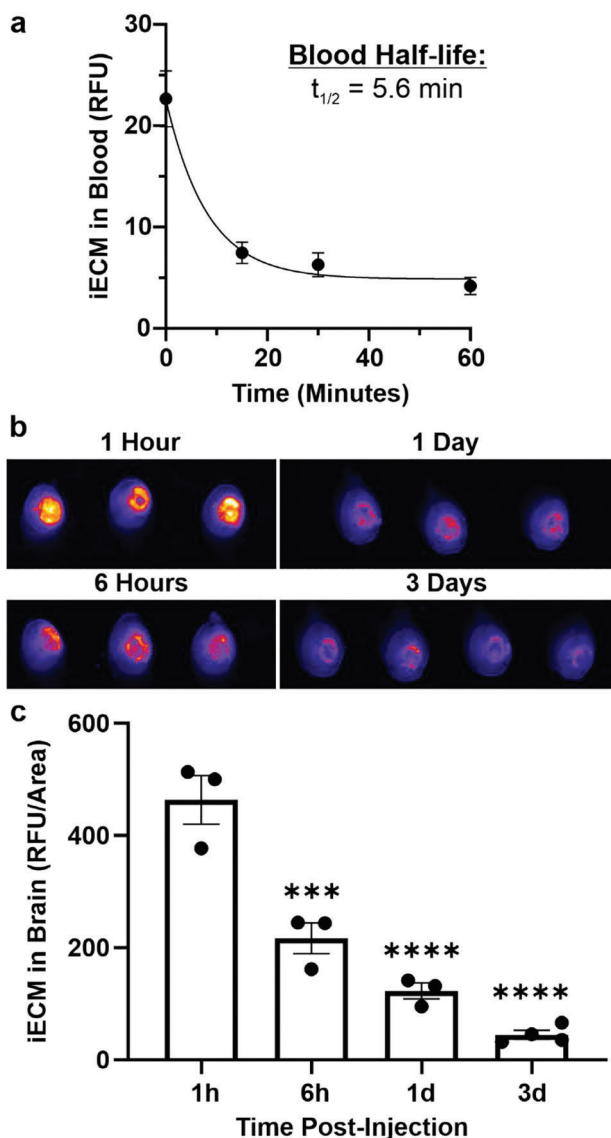
**Figure 3.** iECM is retained in the injury for days. a) Half-life of iECM in the systemic circulation (one phase decay nonlinear curve fit). b) Signal of iECM in the injured brain from 1 h to 3 days post-injection. c) Quantification of iECM signal in the brain ($n = 3–4$, mean $\pm$ SEM, *** $p < 0.001$, **** $p < 0.0001$ via ordinary one-way ANOVA with Dunnett's multiple comparisons test against 1 h).

as endogenous albumin.[26] Additionally, due to the known sex-based differences in vascular permeability after TBI,[27] we performed the study in both male and female mice. iECM was injected 30 min after injury and the two tracers were subsequently injected 30 min after iECM infusion (**Figure 5**a). Animals were perfused and organs were harvested 20 min after tracer injection, and whole brains were imaged to determine the extent of tracer extravasation into the injured region. Analysis of tracer signal in the injured cortex of brain scans shows that after delivery of the iECM, there is a significant 2.5-fold and 1.6-fold reduction in the extravasation of BSA and dextran, respectively, over saline control into the injured tissue (Figure 5b–e). The reduction in tracer extravasation was consistent in both iECM-treated male and female

mice, and no sex-based differences were observed. This suggests iECM can prevent loss of vascular integrity in the brain across a range of molecular sizes of at least 10–66 kDa.

We further investigated this in an in vitro model. The endothelial cells of the BBB are characterized by tight junctions that prevent paracellular transport of proteins and components > 1000 Da and maintain ionic homeostasis across the BBB.[23,25] The integrity of the BBB can also be measured using in vitro methods such as a transendothelial electrical resistance (TEER) assay.[28] We induced inflammation and loss of tight junctions in human umbilical cord vascular endothelial cells (HUVECs) with a 22-h treatment with tumor necrosis factor alpha (TNF$\alpha$),[29] followed by treatment with PBS or iECM for 1 h to allow iECM to bind (Figure 5f). At 24 h after treatment, iECM prevented the loss of resistance across the monolayer compared to the PBS control group (Figure 5g). However, it is not yet determined if this is due to the iECM itself acting as a physical barrier between the endothelial cells or if the material can promote tight junction integrity. Additionally, this assay is limited by its use of HUVECs as opposed to a brain-specific endothelial cell type.

## 2.6. iECM Modulates Pathways of Neuroinflammation

We next investigated the ability of the iECM to impact gene expression using the NanoString nCounter Neuroinflammation panel at days 1 and 5 post-injury. In previous work in a rat acute MI model, iECM modulated gene expression via promoting pathways of neovascularization and modulating the immune and inflammatory response towards pro-repair.[12] The nCounter Neuroinflammation panel is composed of 770 genes that are involved in over 20 pathways of neuroinflammation, including astrogliosis, microglia activation, as well as genes crucial to assessing the integrity of the BBB and endothelial cells. A list of all genes on the panel can be found in the Supporting Information (Table S1, Supporting Information). After CCI and subsequent injection of two doses of either iECM or saline (**Figure 6**a), at day 1 post-injection, we saw 89 differentially expressed genes between treatment groups (Figure 6b, and Table S2 and Figure S3, Supporting Information), and at day 5 post-injection we saw 52 differentially expressed gene between treatment groups (Figure 6c, and Table S3 and Figure S4, Supporting Information). When we evaluate these differentially expressed genes using Gene Ontology (GO) Term enrichment, we found enrichment of pathways associated with cytokine production, immune cell migration, and wound healing at 1-day post-injury (Figure 6d). At day 5 post-injury, we found enrichment for pathways commonly associated with neuroinflammation after TBI, such as viral response pathways and IFN pathways (Figure 6e).

More specifically, at 1 day post-injury, we observed downregulation of proinflammatory cytokines and chemokines such as Ccl2, Ccl5, Ccl7, Ccr2, Cxcl10, Il1r1, and Il1rap. Additionally, modulation of regulators of the complement system such as C3, C3ar1, C5ar, and Serping1 was observed. Activation of the complement system after TBI has been previously shown to have deleterious effects in promoting the expansion of the secondary injury, while there is some evidence that inhibition might provide neuroprotective effects in terms of lesion size and neurological functional measurements.[30] We also show the
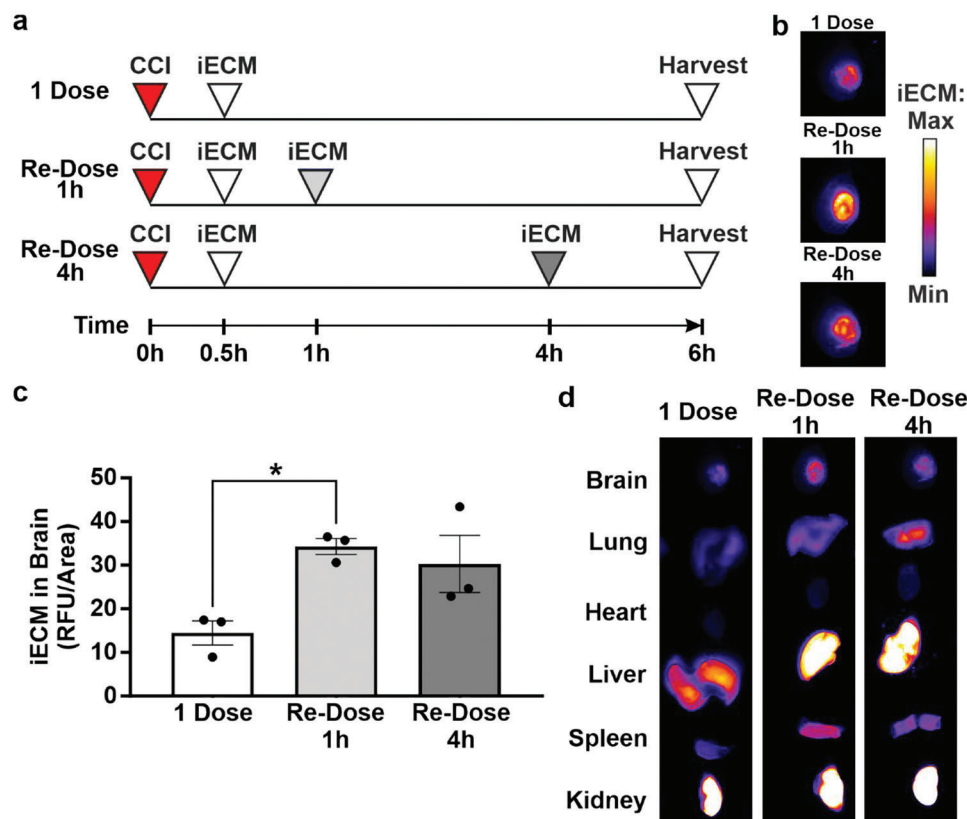
**ADVANCED
SCIENCE NEWS**

www.advancedsciencenews.com

**ADVANCED
HEALTHCARE
MATERIALS**

www.advhealthmat.de

**Figure 4.** Multiple doses of iECM increase material signal in the injury. a) Timeline of multiple-dose study. One cohort received a single dose of iECM 30 min after CCI, while the second and third cohorts received repeat iECM doses at 1 and 4 h, respectively. All organs were harvested at 6 h post-CCI. b) LiCor surface imaging of representative 1 dose and re-dose brains. c) Quantitative analysis of iECM signal in the brains ($n = 3$, mean $\pm$ SEM, * $p <$ 0.05 via ordinary one-way ANOVA with Dunnett's multiple comparisons test against 1 dose). d) Surface scans of representative organs for 1 dose and re-dose cohorts.

downregulation of multiple caspase genes, such as Casp4, 7, and 8. Caspase proteins play an essential role in initiating and executing programmed cell death, with Caspase 7 and 8 having been shown to increase expression after TBI in animal models and human samples.[31,32] Interestingly, Casp8 was expressed specifically in the neurons of human tissue samples post-TBI.[32] This observation is consistent with the significant downregulation of cardiomyocyte apoptosis in the infarct border zone via immunohistochemistry in an acute MI model, implying the protective effects of the iECM across varying models.[12] Finally, we also observed modulation of immune cell markers such as Marco, Cd68, Cd14, Cd33, Cd72, and Cd84, possibly indicating a reduction in immune cell infiltration or activation. When performing GO pathway enrichment on these differentially expressed genes, we find modulation of pathways such as decreased cytokine production, altered migration of various immune cell types, as well as wound healing responses towards pro-repair or anti-inflammation.

At 5 days post-injury, we saw modulation of genes that are associated with BBB integrity, such as downregulation of Cldn5 and Esam. While downregulation of Cldn5 generally indicates poor BBB integrity, there have also been studies showing inhibition of Cldn5 may prove beneficial by improving clearance of fluid in the injury and reducing edema in the sub-acute

phase.[33,34] The downregulation of Esam, on the other hand, is known to be beneficial as its upregulation is associated with increased BBB permeability and increased infiltration of neutrophils.[35,36] The modulation of these genes may play a role in the ability of iECM to promote BBB and vascular integrity. Additionally, we saw upregulation of genes associated with angiogenesis and vascular sprouting, such as Ccl5 (Rantes), Tnf, Tspan18, and Amigo2, which is known to protect vascular ECs that are undergoing oxidative stress.[37–40] This data is reflective of the neovascularization modulation seen in acute MI in which the iECM upregulated genes such as Vegfa, Bmp7, Nrg1, and Fgf2 via NanoString analysis.[12] These mechanisms may provide insight into the interaction between iECM and vascular repair.

In addition to effects on ECs and BBB integrity, at day 5, the iECM modulated genes associated with neuronal protection or neuronal apoptosis. Specifically, we saw the upregulation of Amigo2, Atr, Grin2b Irak3, Bdnf, Sin3a, and Xiap, all of which have been shown to have neuroprotective effects or decrease the apoptosis of neurons.[41–51] Of note is the upregulation of Bdnf, which has previously been investigated as a therapeutic for TBI as it is a known factor that is crucial for healthy neuronal development and maintenance.[47] In addition to promoting survival, it is well established that Bdnf supports neuronal regeneration and differentiation.[52,53] We also observed the upregulation of
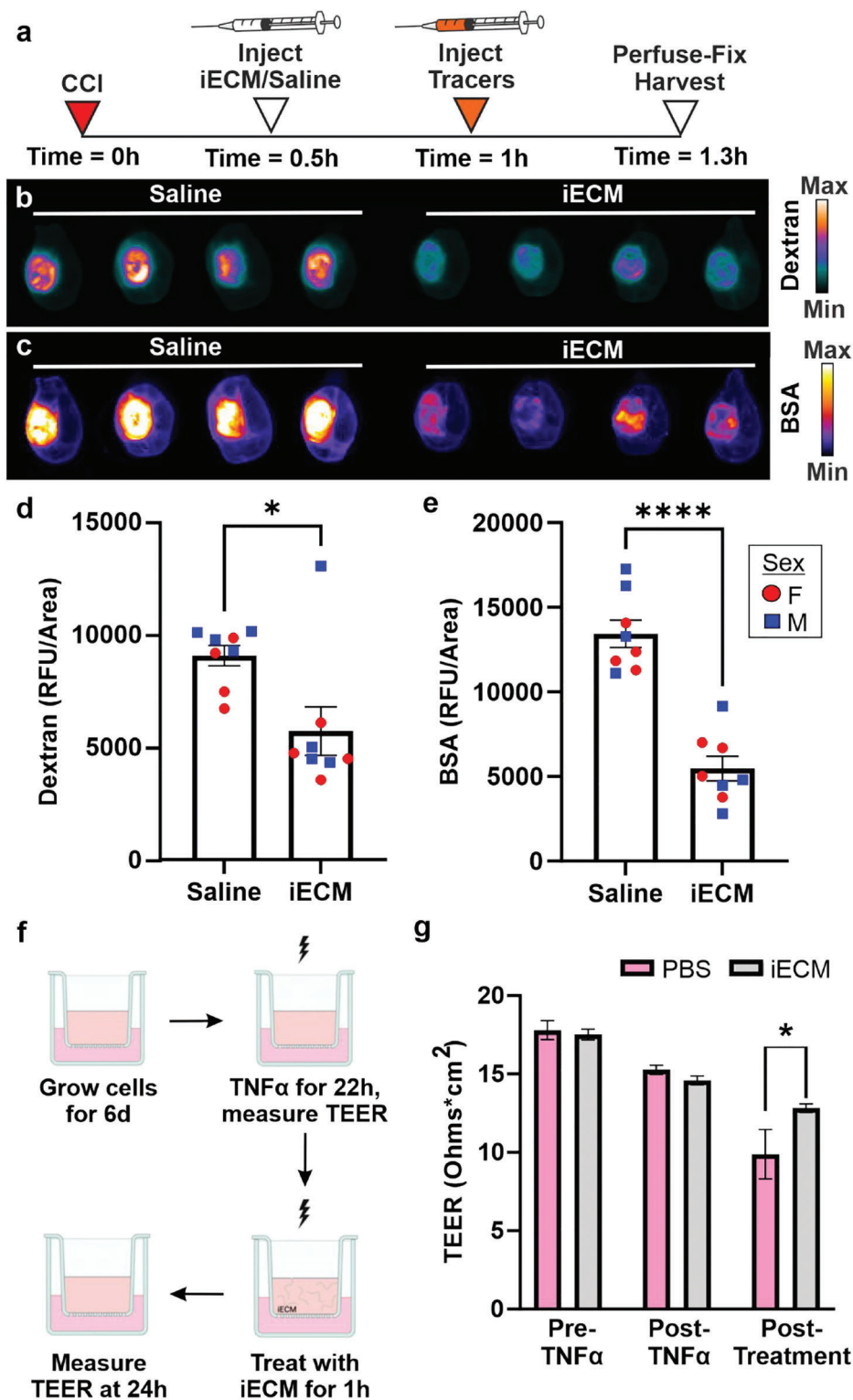
**Figure 5.** iECM localizes to the injured region of the brain and promotes vascular integrity in male and female mice in vivo, and maintains endothelial resistance in vitro. a) Timeline of tracer study. b,c) Representative LiCor Odyssey scans of b) 10 kDa dextran and c) BSA after treatment with iECM or saline control. d,e) iECM reduces the permeability of d) 10 kDa dextran and e) BSA into the injured region of the brain in male (blue square) and female (red circle) mice ($n = 8$, mean $\pm$ SEM, * $p < 0.05$, **** $p < 0.0001$ via unpaired two-tailed $t$-test). f) TEER assay timeline. g) iECM shows a significant increase in TEER at 24 h post-treatment compared to PBS control ($n = 10$–11, mean $\pm$ SEM, * $p < 0.05$ via two-way ANOVA with Sidak's multiple comparisons test).

ADVANCED
SCIENCE NEWS

www.advancedsciencenews.com
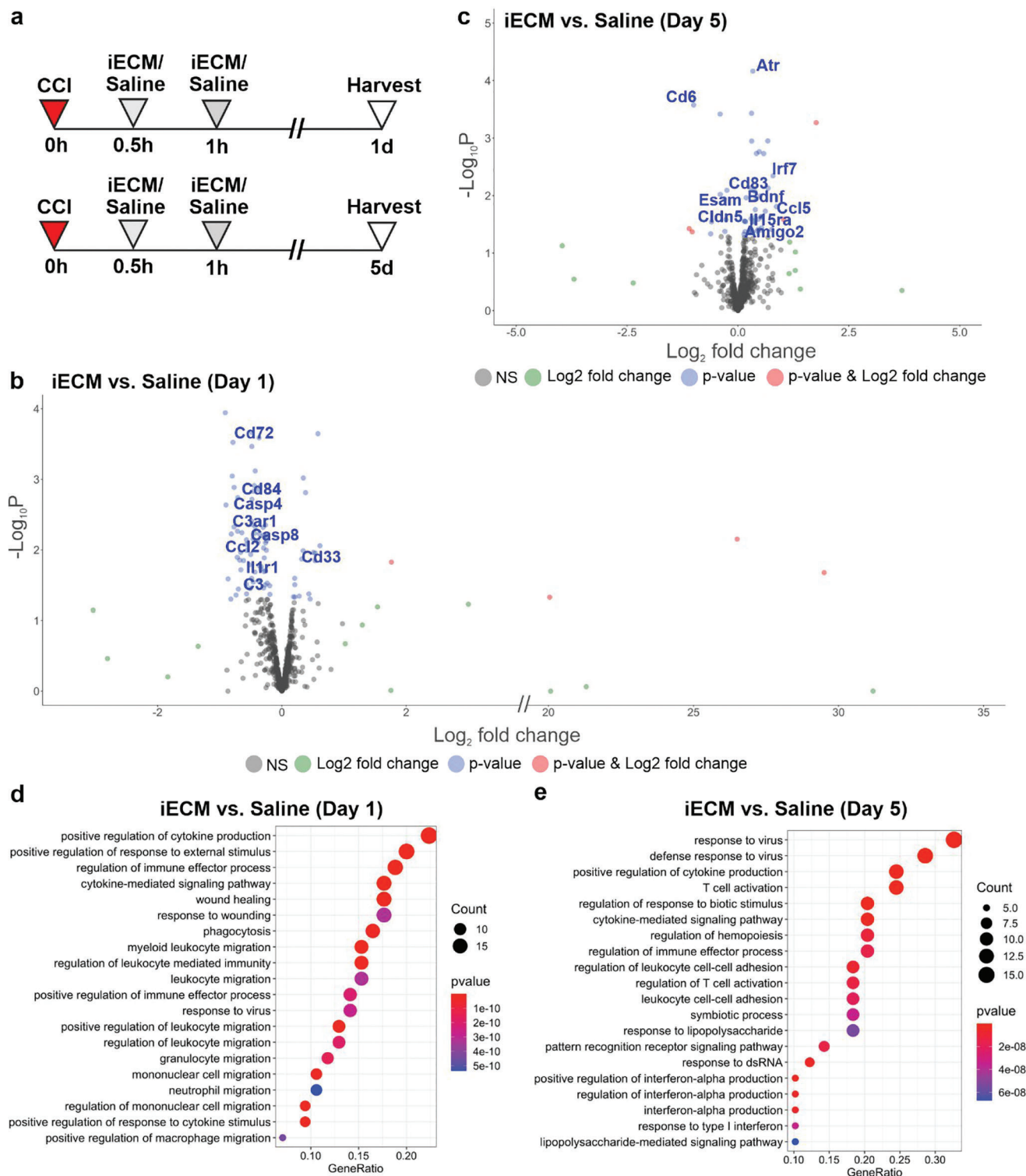
ADVANCED
HEALTHCARE
MATERIALS

www.advhealthmat.de

**Figure 6.** iECM modulates neuroinflammatory pathways at days 1 and 5 post-injury. a) Timeline of study. b,c) Volcano plots of differentially expressed genes at b) days 1 and c) 5 post-injury. d,e) GO dot plots showing enriched pathways of differentially expressed genes at d) days 1 and e) 5 post-injury. N = 5 mice per treatment for each time point.

**ADVANCED
SCIENCE NEWS**

www.advancedsciencenews.com

**ADVANCED
HEALTHCARE
MATERIALS**

www.advhealthmat.de

Sin3a, which has been shown to be important for cognition and memory and is associated with hippocampal function.[42] As ROS generation is a key mechanism by which the secondary injury of TBI spreads and damages neurons and other brain cell types, it's important to point out the modulation of genes involved in oxidative stress. The iECM downregulated Irf6 and Osgin1, both of which are known to be upregulated during times of oxidative stress.[51,54] While these data together support a role for iECM in neuronal protection and neurogenesis, phenotypes such as neuronal proliferation and axonal sprouting are not exhibited until a week or more after injury.[55] Therefore, further investigation into the impact of iECM on neuronal protection and regeneration is warranted.

Additionally, we point out that the iECM was also shown to modulate certain markers of microglia or astrocyte activation involving Cd6, Cd86, Cd83, Il15ra, Irf7, Tmem204, and Suz12. It is important to note that by day 5 post-injection, the iECM should be degraded and largely absent from the injured brain. Taken together, this may suggest that iECM can play a role in the suppression of proinflammatory pathways in the acute phase post-injury that results in neuroprotection and endothelial cell survival or proliferation within the first 5 days post-injury.

## 3. Conclusion

TBI is among the leading causes of disability in the US and worldwide.[56] While the primary injury can only be prevented, the progressive loss of neuronal tissue during the secondary injury is an opportunity for therapeutic intervention. Injury to the BBB plays a large role in exacerbating the secondary injury and preventing, halting, or reversing BBB dysfunction is a promising therapeutic target for preventing tissue loss. Previous applications of the iECM have shown promise for promoting the repair of endothelial cell dysfunction and improving cardiac function in small and large pre-clinical models of acute myocardial infarction.[12] While the iECM has been characterized previously in vitro and has undergone hemocompatibility studies in vivo,[12] in this work, we performed further characterization of the iECM in a mouse model of TBI.

In this study, we have shown that we can deliver an infusible ECM-derived biomaterial through i.v. delivery with localization to the injured brain in an acute model of TBI. The localization and retention of the material are dose-dependent, and multiple doses can further increase accumulation in the brain, although given the limited volume that can be injected into the bloodstream in mice and the inability to directly scale dosing to a large animal (or human), dosing optimization (both low and high doses) will need to be optimized in a large animal model. We also found that the iECM is able to reduce vascular permeability in the brain in vivo and improve the TEER of a HUVEC monolayer in vitro. Gene expression analyses elucidated the ability of the iECM to modulate key pathways of neuroinflammation that are associated with response to TBI. Specifically, the iECM mitigates inflammation within the first day of injury, which may result in the modulation of angiogenic and BBB integrity pathways. This early mitigation of the inflammatory response is hypothesized to be linked to the ability of the iECM to reduce vascular permeability when applied acutely after injury, possibly lessening the extent of secondary injury.

## 4. Experimental Section

*Infusible Extracellular Matrix Preparation*: The liquid precursor of the myocardial matrix hydrogel was generated based on previously described protocols.[57,58] Briefly, hearts were harvested from adult Yorkshire farm pigs (30–45 kg), and the LV myocardium was isolated. Tissue was first processed to remove major vessels and connective tissue. The remaining tissue was minced. The tissue was decellularized in 1% sodium dodecyl sulfate (SDS) in phosphate buffer saline (PBS) for 4–5 days. After decellularization, there was 24 h of water rinsing to remove any remaining detergent. The material was then lyophilized and milled into a fine powder and then partially enzymatically digested using pepsin in 0.1 M hydrochloric acid at a concentration of 10 mg ml$^{-1}$ ECM powder and 1 mg ml$^{-1}$ pepsin for at least 48 h. Next, the material was neutralized using sodium hydroxide and buffered to match in vivo conditions, which yielded a liquid myocardial matrix. Finally, the myocardial matrix was diluted to 6 mg ml$^{-1}$ using PBS.

Next, the liquid myocardial matrix was centrifuged at 15000 RCF at 4 °C for 45 min to separate the high and low molecular weight components. The supernatant (low molecular weight components, iECM) was isolated from the insoluble pellet. The pellet was then rinsed with PBS, and centrifugation was repeated to increase the yield of iECM. To adjust the concentration of salts, the iECM was dialyzed over 48 h at 4 °C in 0.5× PBS, 0.25× PBS, and then two times in deionized water (with each solution being replaced approximately every 12 h), and then lyophilized. After dialysis, the iECM was resuspended at a high concentration of 16 mg mL$^{-1}$ in 1× PBS and passed through 0.22 μm syringe filters (Millipore) into sterile test tubes. It was then lyophilized, weighed, and stored at −80 °C for future use. Once ready for injection, the iECM was then resuspended to the appropriate concentration in sterile water at least 30 min before injection and placed on ice. For fluorescently labeled iECM or trilysine, the material was conjugated at room temperature for a minimum of 1 h before injection with 10 mg mL$^{-1}$ of either VivoTag 750 (PerkinElmer, dilution 1:1000) or AlexaFluor 568 (Invitrogen, dilution 1:100) as previously described.[12]

*Infusible Extracellular Matrix Characterization and Quality Control*: The iECM was characterized as previously described.[12] In short, the iECM peptide size and distribution were visualized through SDS-PAGE using a 4–12% Bis-Tris gel NuPage Kit (Invitrogen). The controls were a rat tail collagen type I, the full ECM hydrogel counterpart from the same biological batch of hearts, and an Abcam Prestained Protein Ladder Broad molecular weight ranging from 10–245 kDa (ab116028). Double-stranded DNA was quantified for the iECM. Aliquots were digested with Proteinase-K, isolated with a NucleoSpin kit, and quantified using a PicoGreen fluorescent reporter. Sulfated glycosaminoglycans (sGAGs) for iECM were quantified using a 1,9-dimethyl methylene blue (DMMB) assay and compared against chondroitin sulfate standards. Complex viscosity was measured on a TA Instruments AR-G2 rheometer using a shear rate sweep test from 0.1 to 1000 s$^{-1}$. The iECM was resuspended, and 200 μL was measured at a gap distance of 500 μm at 25 °C. Optical properties (absorbance) were measured as previously described. An absorbance scan was performed on a Spark microplate reader (Tecan) with 5 nm steps from 230 to 1000 nm, temperature maintained at 25 °C, using iECM at 10 mg ECM/mL alongside saline as a control. Transmittance was calculated from absorbance using the equation; transmittance = 10^(2 − absorbance). Cryogenic transmission electron microscopy (CryoTEM) samples were prepared via a vitrification robot (Vitrobot Mark IV, ThermoFisher). Lacey carbon 300 mesh copper TEM grids were purchased from EMS. TEM grids were glow discharged (K950X, Emitech) for 45 s with a 20-mA current before vitrification. For sample vitrification, 4 uL iECM solution at 10 mg ECM per mL was pipetted onto the TEM grid and placed inside the Vitrobot chamber, which was maintained at 4 °C and 95% relative humidity. The grid was blotted immediately with filter paper to remove the excess solution with a blot time of 4 s, a blot force of 4, and subsequently plunge-frozen in liquid ethane. The vitrified samples were transferred to and stored in liquid nitrogen. Samples were imaged using a Talos Artica (FEI) (maintained at ≤ −170 °C) operating at 200 kV equipped with a Falcon 4i Direct Electron Detector (ThermoFisher). Images were collected using EPU (Version 3.2, ThermoFisher). Exposures were taken with Data Acquisition preset (150k×

magnification, 0.95 Andstrom/pixel, Dose: ≈40–50 electron/Angstrom^2) and were automatically motion corrected within EPU.

*Surgical Procedures*: All described mouse procedures were approved by Institutional Animal Care and Use Committee (IACUC) at the University of California San Diego, Animal Welfare Assurance number D16-00020. 8–10-week-old female or male C57BL/6J mice (Jackson Labs) were secured in a stereotaxic frame under 2.5% isoflurane anesthesia, and a 5-mm-diameter craniotomy was performed above the right cortex. Controlled cortical impact (CCI) was performed with a 2-mm-diameter stainless steel piston tip at a velocity of 3 m s$^{-1}$ to a depth of 2 mm and 100 ms dwell time using an ImpactOne (Leica Biosystems) at a location of $2.0 \pm 0.5$ mm caudal and $2.0 \pm 0.5$ mm right of bregma. For in vivo vascular permeability studies, bovine serum albumin (Sigma) labeled with VivoTag 750 fluorophore and 10 kDa dextran (Sigma) labeled with AlexaFluor 680 were injected intravenously at a tracer concentration of 5 mg kg$^{-1}$. Brains and satellite organs used for immunohistochemistry and histology were harvested after perfusion fixation at times indicated. Animals used for gene expression analyses were briefly perfused with cold PBS, and organs were harvested and immediately frozen.

*Tissue Processing*: Fluorescence signals from whole organs were imaged on a LiCor Odyssey. To perform immunohistochemistry, fixed organs were equilibrated in 30% w/v sucrose-PBS overnight and subsequently frozen in TissueTek OCT. Ten-micron frozen coronal sections were collected within the injury region and subsequently used for immunohistochemistry. For CD31 staining, tissues were blocked for 1 h in 0.1% TritonX-100, 2% bovine serum albumin, and 5% serum of secondary antibody. CD31 primary antibody (BD 553370) was applied to tissues at 2.5 µg mL$^{-1}$ concentration overnight at 4 °C. Following three 1× PBS wash steps, Gt anti-RT 647 secondary antibodies (Thermo A-21247) diluted 1:500 and Hoechst 33342 (Thermo) diluted 1:1000 were incubated for 1 h at room temperature. Finally, tissues were washed with 1× PBS and mounted with Fluoromount-G (Southern Biotech). Images were obtained using a Nikon Eclipse Ti2 microscope fitted with a Hamamatsu Orca-Flash 4.0 digital camera. The same exposure and LED intensity settings were used across all images for direct comparison.

*TEER Assay*: Human umbilical vein endothelial cells (HUVECs) were cultured on transwell permeable supports for 6 days in endothelial cell growth medium-2 (PromoCell). On the sixth day, in some sample groups, TNFα was added to the media at a concentration of 100 ng mL$^{-1}$ for 22 h. After 22 h of TNFα treatment, 100 µL of PBS or iECM at a concentration of 10 mg mL$^{-1}$ were doped into the top compartment of the transwell and allowed to incubate for 1 h. After 1 h of treatment with PBS or iECM, the top compartment of the transwell was replaced with fresh media and allowed to incubate for 24 h. Transendothelial electrical resistance (TEER) measurements were taken with an EVOM2 Meter (World Precision Instruments) before TNFα treatment, immediately after TNFα treatment, and 24 h post-treatment with PBS or iECM. TEER was determined via the following equation: $\Omega cm^2 = (\Omega_{sample} - \Omega_{blank}) \times transwell\ surface\ area$.

*NanoString Multiplex Gene Expression Analysis*: RNA was isolated from the injured region of the brain using the BeadBug 6 tissue homogenizer and the Qiagen RNeasy Tissue Mini Kit. The NanoString nCounter MAX Analysis System[59,60] with nCounter Neuroinflammation Panel (Mouse) allowed for the multiplexed assessment of over 700 genes (see Table S1, Supporting Information for full gene list). Samples were processed according to manufacturer instructions. In brief, RNA sample concentrations were measured on a Qubit 3.0 Fluorometer with a Qubit RNA HS Assay kit. 70 µL of hybridization buffer was mixed with Immunology Panel Reporter CodeSet solution, and 8 µL of this master mix was mixed in a separate reaction vessel with 50–100 ng of RNA per tissue sample and RNA-free water up to 13 µL total. 2 µL of Capture ProbeSet was added to each vessel, mixed, and placed on a thermocycler at 65 °C for 16–48 h before being maintained at 4 °C for less than 24 h. NanoString nCounter Prep Station performed automated fluidic sample processing to purify and immobilize hybridized samples to the cartridge surface. Digital barcode reads were analyzed by NanoString nCounter Digital Analyzer. Results were analyzed by manufacturer nSolver Analysis Software 4.0 and custom R scripts.

*Statistical Analysis*: In vivo LiCor dose-dependent accumulation, degradation, and re-dose results were compared using one-way ANOVA

with Dunnett's correction. In vitro TEER assay results were compared using two-way ANOVA with Sidak's Correction. In vivo tracer permeability assay was compared between iECM and saline control groups using an unpaired two-tailed *t*-test. Significance was accepted at *p*-value < 0.05. Data were reported as mean ± SEM. GraphPad Prism (9.2.0) was used for statistics. Gene expression normalization and differential expression were analyzed by the NanoStringDiff package with significance at a *p*-value < 0.05.[61] Heatmap was displayed with the pheatmap package ([Software] KRpPh). Gene enrichment analysis was performed with the clusterprofiler package[62] and KEGG pathway images created with the Pathview package.[63]

## Supporting Information

Supporting Information is available from the Wiley Online Library or from the author.

## Conflict of Interest

K.L.C. is a co-founder, board member, and consultant and holds an equity interest in Ventrix Bio, Inc. All other authors have reported that they have no relationships relevant to the contents of this paper disclosure.

## Data Availability Statement

The data that support the findings of this study are available from the corresponding author upon reasonable request.

[1] U. S. D. of H. and H. Services, Centers for Disease Control and Prevention, *Surveillance Report of Traumatic Brain Injury-Related Deaths by Age Group, Sex, and Mechanism of Injury—United States*, **2018**.

**ADVANCED
SCIENCE NEWS**

www.advancedsciencenews.com

**ADVANCED
HEALTHCARE
MATERIALS**

www.advhealthmat.de

[2] Centers for Disease Control and Prevention, Traumatic Brain Injury, Health Disparities and TBI, https://www.cdc.gov/traumaticbraininjury/health-disparities-tbi.html (accessed: March **2022**).

[3] A. C. McKee, D. H. Daneshvar, *Handb. Clin. Neurol.* **2015**, *127*, 45.

[4] M. Prins, T. Greco, D. Alexander, C. C. Giza, *Dis. Models Mech.* **2013**, *6*, 1307.

[5] B. J. Boyd, A. Galle, M. Daglas, J. V. Rosenfeld, R. Medcalf, *J. Drug Targeting* **2015**, *23*, 847.

[6] M. Kuriakose, D. Younger, A. R. Ravula, E. Alay, K. V. Rama Rao, N. Chandra, *Sci. Rep.* **2019**, *9*, 7717.

[7] M. K. Baskaya, A. M. Rao, A. Dogan, D. Donaldson, R. J. Dempsey, *Neurosci. Lett.* **1997**, *226*, 33.

[8] J. L. Ungerleider, T. D. Johnson, M. J. Hernandez, D. I. Elhag, R. L. Braden, M. Dzieciatkowska, K. G. Osborn, K. C. Hansen, E. Mahmud, K. L. Christman, *JACC Basic Transl. Sci.* **2016**, *1*, 32.

[9] J. W. Wassenaar, R. Gaetani, J. J. Garcia, R. L. Braden, C. G. Luo, D. Huang, A. N. DeMaria, J. H. Omens, K. L. Christman, *J. Am. Coll. Cardiol.* **2016**, *67*, 1074.

[10] M. E. Carnes, G. D. Pins, *Bioengineering* **2020**, *7*, 85.

[11] B. M. Sicari, J. P. Rubin, C. L. Dearth, M. T. Wolf, F. Ambrosio, M. Boninger, N. J. Turner, D. J. Weber, T. W. Simpson, A. Wyse, E. H. P. Brown, J. L. Dziki, L. E. Fisher, S. Brown, S. F. Badylak, *Sci. Transl. Med.* **2014**, *6*, 234ra58.

[12] M. T. Spang, R. Middleton, M. Diaz, J. Hunter, J. Mesfin, A. Banka, H. Sullivan, R. Wang, T. S. Lazerson, S. Bhatia, J. Corbitt, G. D'Elia, G. Sandoval-Gomez, R. Kandell, M. A. Vratsanos, K. Gnanasekaran, T. Kato, S. Igata, C. Luo, K. G. Osborn, N. C. Gianneschi, O. Eniola-Adefeso, P. Cabrales, E. J. Kwon, F. Contijoch, R. R. Reeves, A. N. DeMaria, K. L. Christman, *Nat. Biomed. Eng.* **2022**, *7*, 94.

[13] Y. Wu, J. Wang, Y. Shi, H. Pu, R. K. Leak, A. K. F. Liou, S. F. Badylak, Z. Liu, J. Zhang, J. Chen, L. Chen, *Cell Transplant.* **2017**, *26*, 1224.

[14] Y. J. Kim, *J. Emerg. Nurs.* **2011**, *37*, 328.

[15] J. A. DeQuach, S. H. Yuan, L. S. B. Goldstein, K. L. Christman, *Tissue Eng., Part A* **2011**, *17*, 2583.

[16] C. J. Medberry, P. M. Crapo, B. F. Siu, C. A. Carruthers, M. T. Wolf, S. P. Nagarkar, V. Agrawal, K. E. Jones, J. Kelly, S. A. Johnson, S. S. Velankar, S. C. Watkins, M. Modo, S. F. Badylak, *Biomaterials* **2013**, *34*, 1033.

[17] T. L. Sellaro, A. K. Ravindra, D. B. Stolz, S. F. Badylak, *Tissue Eng.* **2007**, *13*, 2301.

[18] M. C. McCabe, A. J. Saviola, K. C. Hansen, *J. Proteome Res.* **2023**, *22*, 790.

[19] J. H. Traverse, T. D. Henry, N. Dib, A. N. Patel, C. Pepine, G. L. Schaer, J. A. DeQuach, A. M. Kinsey, P. Chamberlin, K. L. Christman, *JACC Basic Transl. Sci.* **2019**, *4*, 659.

[20] P. K. Dash, J. Zhao, N. Kobori, J. B. Redell, M. J. Hylin, K. N. Hood, A. N. Moore, *J. Neurosci.* **2016**, *36*, 2809.

[21] J. J. Donkin, R. Vink, *Curr. Opin. Neurol.* **2010**, *23*, 293.

[22] D. Shlosberg, M. Benifla, D. Kaufer, A. Friedman, *Nat. Rev. Neurol.* **2010**, *6*, 393.

[23] Z.-H. Liu, N.-Y. Chen, P. Tu, C.-T. Wu, S.-C. Chiu, Y.-C. Huang, S.-N. Lim, P. K. Yip, *Iran. J. Med. Sci.* **2020**, *21*, 6291.

[24] K. S. Prabhakara, D. J. Kota, G. H. Jones, A. K. Srivastava, C. S. Cox, S. D. Olson, *Mol. Ther.* **2018**, *26*, 2152.

[25] H. S. Sharma, S. Zimmermann-Meinzingen, C. E. Johanson, *Ann. N. Y. Acad. Sci.* **2010**, *1199*, 125.

[26] H. Kadry, B. Noorani, L. Cucullo, *Fluids Barriers CNS* **2020**, *17*, 69.

[27] V. N. Bharadwaj, C. Copeland, E. Mathew, J. Newbern, T. R. Anderson, J. Lifshitz, V. D. Kodibagkar, S. E. Stabenfeldt, *Tissue. Eng., Part A* **2020**, *26*, 688.

[28] B. Srinivasan, A. R. Kolli, M. B. Esch, H. E. Abaci, M. L. Shuler, J. J. Hickman, *SLAS Technol.* **2015**, *20*, 107.

[29] K. Miyazaki, K. Hashimoto, M. Sato, M. Watanabe, N. Tomikawa, S. Kanno, Y. Kawasaki, N. Momoi, M. Hosoya, *Pediatr. Res.* **2017**, *81*, 942.

[30] A. Hammad, L. Westacott, M. Zaben, *J. Neuroinflammation* **2018**, *15*, 24.

[31] S. F. Larner, D. M. McKinsey, R. L. Hayes, K. K. W. Wang, *J. Neurochem.* **2005**, *94*, 97.

[32] X. Zhang, S. H. Graham, P. M. Kochanek, D. W. Marion, P. D. Nathaniel, S. C. Watkins, R. S. B. Clark, *FASEB J.* **2003**, *17*, 1367.

[33] M. Campbell, F. Hanrahan, O. L. Gobbo, M. E. Kelly, A.-S. Kiang, M. M. Humphries, A. T. H. Nguyen, E. Ozaki, J. Keaney, C. W. Blau, C. M. Kerskens, S. D. Cahalan, J. J. Callanan, E. Wallace, G. A. Grant, C. P. Doherty, P. Humphries, *Nat. Commun.* **2012**, *3*, 849.

[34] C. Greene, N. Hanley, M. Campbell, *Fluids Barriers CNS* **2019**, *16*, 3.

[35] S. Butz, D. Vestweber, in *Adhesion Molecules: Function and Inhibition* (Ed: K. Ley), Birkhäuser, Basel **2007**, p. 253.

[36] S. M. Stamatovic, A. M. Johnson, R. F. Keep, A. V. Andjelkovic, *Tissue Barriers* **2016**, *4*, 1154641.

[37] S. Hossain, M. U. Ahmed, S. Alam, A. Watanabe, A. Harashima, H. Yonekura, H. Yamamoto, *Int. J. Biosci., Biochem. Bioinf.* **2012**, *2*, 1.

[38] N. Suffee, B. Richard, H. Hlawaty, O. Oudar, N. Charnaux, A. Sutton, *Biochem. Soc. Trans.* **2011**, *39*, 1649.

[39] R. C. A. Sainson, D. A. Johnston, H. C. Chu, M. T. Holderfield, M. N. Nakatsu, S. P. Crampton, J. Davis, E. Conn, C. C. W. Hughes, *Blood* **2008**, *111*, 4997.

[40] G. X. Li, S. Zhang, R. Liu, B. Singh, S. Singh, D. I. Quinn, G. Crump, P. S. Gill, *Biol. Open* **2021**, *10*, 050096.

[41] A. Mammis, T. K. McIntosh, A. H. Maniker, *Surg. Neurol.* **2009**, *71*, 527.

[42] M. Bridi, H. Schoch, C. Florian, S. G. Poplawski, A. Banerjee, J. D. Hawk, G. S. Porcari, C. Lejards, C.-G. Hahn, K.-P. Giese, R. Havekes, N. Spruston, T. Abel, *JCI Insight* **2020**, *5*, 92385.

[43] T. West, M. Stump, G. Lodygensky, J. J. Neil, M. Deshmukh, D. M. Holtzman, *ASN Neuro* **2009**, *1*, AN20090005.

[44] Z. Wang, Z. Wang, A. Wang, J. Li, J. Wang, J. Yuan, X. Wei, F. Xing, W. Zhang, N. Xing, *J. Neuroinflammation* **2022**, *19*, 51.

[45] A. Laeremans, J. Nys, W. Luyten, R. D'Hooge, M. Paulussen, L. Arckens, *Brain Struct. Funct.* **2013**, *218*, 123.

[46] F. M. S. Gurgis, W. Ziaziaris, L. Munoz, *Mol. Pharmacol.* **2014**, *85*, 345.

[47] M. Miranda, J. F. Morici, M. B. Zanoni, P. Bekinschtein, *Front. Cell. Neurosci.* **2019**, *13*, 363.

[48] M. German-Fattal, F. Lecerf, F. Sabbagh, P. Maurois, J. Durlach, P. Bac, *Biomed. Pharmacother.* **2008**, *62*, 264.

[49] D. Appel, R. Hummel, M. Weidemeier, K. Endres, C. Gölz, M. K. E. Schäfer, *Front. Cell Dev. Biol.* **2021**, *9*, 661462.

[50] C. Lyu, Y. Zhang, M. Gu, Y. Huang, G. Liu, C. Wang, M. Li, S. Chen, S. Pan, Y. Gu, *Front. Cell. Neurosci.* **2018**, *12*, 504.

[51] Y. Lin, D. Xu, X. Li, C. Liu, X. Liu, S. Huang, Y. Huang, X. Liu, *Cell. Mol. Neurobiol.* **2016**, *36*, 27.

[52] Z. Shi, Z. Fan, H. Zhang, S. Li, H. Yuan, J. Tong, *J. Orthop. Surg. Res.* **2022**, *17*, 172.

[53] M. Wurzelmann, J. Romeika, D. Sun, *Neural Regener. Res.* **2017**, *12*, 7.

[54] M. S. Brennan, M. F. Matos, K. E. Richter, B. Li, R. H. Scannevin, *Sci. Rep.* **2017**, *7*, 42054.

[55] S. Y. Sophie, A. Veeravagu, G. Grant, in *Translational Research in Traumatic Brain Injury* (Eds: D. Laskowitz, G. Grant), CRC Press/Taylor And Francis Group, Boca Raton, FL **2016**.

[56] A. I. R. Maas, D. K. Menon, P. D. Adelson, N. Andelic, M. J. Bell, A. Belli, P. Bragge, A. Brazinova, A. Büki, R. M. Chesnut, G. Citerio, M. Coburn, D. J. Cooper, A. T. Crowder, E. Czeiter, M. Czosnyka, R. Diazarrastia, R. L. Gruen, D. Gupta, J. A. Hartings, et al., *Lancet Neurol* **2017**, *16*, 987.

**ADVANCED
SCIENCE NEWS**

www.advancedsciencenews.com

**ADVANCED
HEALTHCARE
MATERIALS**

www.advhealthmat.de

[57] J. M. Singelyn, J. A. DeQuach, S. B. Seif-Naraghi, R. B. Littlefield, P. J. Schup-Magoffin, K. L. Christman, *Biomaterials* **2009**, *30*, 5409.

[58] J. L. Ungerleider, T. D. Johnson, N. Rao, K. L. Christman, *Methods* **2015**, *84*, 53.

[59] L. Jardine, S. Wiscombe, G. Reynolds, D. McDonald, A. Fuller, K. Green, A. Filby, I. Forrest, M.-H. Ruchaud-Sparagano, J. Scott, M. Collin, M. Haniffa, A. J. Simpson, *Nat. Commun.* **2019**, *10*, 1999.

[60] S. Hussain, C. G. Johnson, J. Sciurba, X. Meng, V. P. Stober, C. Liu, J. M. Cyphert-Daly, K. Bulek, W. Qian, A. Solis, Y. Sakamachi, C. S. Trempus, J. J. Aloor, K. M. Gowdy, W. M. Foster, J. W. Hollingsworth, R. M. Tighe, X. Li, M. B. Fessler, S. Garantziotis, *Elife* **2020**, *9*, 50458.

[61] H. Wang, C. Horbinski, H. Wu, Y. Liu, S. Sheng, J. Liu, H. Weiss, A. J. Stromberg, C. Wang, *Nucleic Acids Res.* **2016**, *44*, 151.

[62] G. Yu, L.-G. Wang, Y. Han, Q.-Y. He, *OMICS* **2012**, *16*, 284.

[63] W. Luo, C. Brouwer, *Bioinformatics* **2013**, *29*, 1830.

**2300782 (12 of 12)**